

Properties of focused Laguerre-Gaussian beam propagating in anisotropic ocean turbulence

Xinguang Wang(王新光), Yangbin Ma(马洋斌), Qiujie Yuan(袁邱杰), Wei Chen(陈伟), Le Wang(王乐), and Shengmei Zhao(赵生妹)

Citation: Chin. Phys. B, 2024, 33 (**2**): 024208. DOI: 10.1088/1674-1056/ad053c
Journal homepage: http://cpb.iphy.ac.cn; http://iopscience.iop.org/cpb

What follows is a list of articles you may be interested in

Spatial quantum coherent modulation with perfect hybrid vector vortex beam based on atomic medium

Yan Ma(马燕), Xin Yang(杨欣), Hong Chang(常虹), Xin-Qi Yang(杨鑫琪), Ming-Tao Cao(曹明涛), Xiao-Fei Zhang(张晓斐), Hong Gao(高宏), Rui-Fang Dong(董瑞芳), and Shou-Gang Zhang(张首刚)
Chin. Phys. B, 2024, 33 (**2**): 024204. DOI: 10.1088/1674-1056/ad0f86

Terahertz quasi-perfect vortex beam with integer-order and fractional-order generated by spiral spherical harmonic axicon

Si-Yu Tu(涂思语), De-Feng Liu(刘德峰), Jin-Song Liu(刘劲松), Zhen-Gang Yang(杨振刚), and Ke-Jia Wang(王可嘉)
Chin. Phys. B, 2024, 33 (**1**): 014211. DOI: 10.1088/1674-1056/acf91c

Ultraviolet metalens and metalens array of focused vortex beams

Jinping Zhang(张金平), Yan Wang(王焱), Huan Yuan(袁欢), Zehao Wang(王泽豪), Yang Deng(邓阳),Chengzhi Huang(黄承志), Jiagui Wu(吴加贵), and Junbo Yang(杨俊波)
Chin. Phys. B, 2023, 32 (**6**): 064206. DOI: 10.1088/1674-1056/ac9d87

Propagation and focusing characteristics of the Bessel-Gaussian beam with the spiral phase term of new power-exponent-phase

Aotian Wang(王傲天), Lianghong Yu(於亮红), Jinfeng Li(李进峰), and Xiaoyan Liang(梁晓燕)
Chin. Phys. B, 2023, 32 (**4**): 044201. DOI: 10.1088/1674-1056/acb1fe

Generation of elliptical airy vortex beams based on all-dielectric metasurface

Xiao-Ju Xue(薛晓菊), Bi-Jun Xu(徐弼军), Bai-Rui Wu(吴白瑞), Xiao-Gang Wang(汪小刚), Xin-Ning Yu(俞昕宁), Lu Lin(林露), and Hong-Qiang Li(李宏强)
Chin. Phys. B, 2023, 32 (**2**): 024215. DOI: 10.1088/1674-1056/ac7cd0

Properties of focused Laguerre–Gaussian beam propagating in anisotropic ocean turbulence

Xinguang Wang(王新光)[1,†], Yangbin Ma(马洋斌)[1], Qiujie Yuan(袁邱杰)[1], Wei Chen(陈伟)[1], Le Wang(王乐)[2], and Shengmei Zhao(赵生妹)[2,3,4]

[1] *College of Science, Nanjing University of Posts and Telecommunications, Nanjing* 210003, *China*
[2] *Institute of Signal Processing and Transmission, Nanjing University of Posts and Telecommunications, Nanjing* 210003, *China*
[3] *Key Lab of Broadband Wireless Communication and Sensor Network Technology (Ministry of Education), Nanjing University of Posts and Telecommunications, Nanjing* 210003, *China*
[4] *National Laboratory of Solid State Microstructures, Nanjing University, Nanjing* 210093, *China*

(Received 10 August 2023; revised manuscript received 9 October 2023; accepted manuscript online 20 October 2023)

We analyze the properties of a focused Laguerre–Gaussian (LG) beam propagating through anisotropic ocean turbulence based on the Huygens–Fresnel principle. Under the Rytov approximation theory, we derive the analytical formula of the channel capacity of the focused LG beam in the anisotropic ocean turbulence, and analyze the relationship between the capacity and the light source parameters as well as the turbulent ocean parameters. It is found that the focusing mirror can greatly enhance the channel capacity of the system at the geometric focal plane in oceanic turbulence. The results also demonstrate that the communication link can obtain high channel capacity by adopting longer beam wavelength, greater initial beam waist radius, and larger number of transmission channels. Further, the capacity of the system increases with the decrease of the mean squared temperature dissipation rate, temperature-salinity contribution ratio and turbulence outer scale factor, and with the increase of the kinetic energy dissipation rate per unit mass of fluid, turbulence inner scale factor and anisotropy factor. Compared to a Hankel–Bessel beam with diffraction-free characteristics and unfocused LG beam, the focused LG beam shows superior anti-turbulence interference properties, which provide a theoretical reference for research and development of underwater optical communication links using focused LG beams.

Keywords: vortex beam, orbital angular momentum, focusing mirror, anisotropic turbulence

PACS: 42.25.Bs, 42.68.Ay, 42.68.Xy **DOI:** 10.1088/1674-1056/ad053c

1. Introduction

Owing to the orthogonality and completeness of orbital angular momentum (OAM),[1–3] which could theoretically form an infinite-dimensional Hilbert space, there are an infinite number of quantum bit bases that can be loaded with information. The carrier wave carrying OAM is often referred to as vortex beams that have a wide range of applications in optical tweezers, particle manipulation, and quantum entanglement.[4–7] In particular, the efficiency and performance of vortex beam-based communication systems can be greatly improved in that the number of signal bits each photon carries is $\log_2 N$,[8] where N is the number of OAM modes that can be available for information mulplexing, which is one of the research hotspots in the field of free-space optical communication.[9–11]

It is worth noting that there appears to be distortion of the signal OAM mode and crosstalk between different energy states of adjacent OAM modes during the transmission of the vortex beam in turbulent medium, reducing the channel capacity of the OAM information transmission system severely, where the effect of refractive index fluctuation of turbulent medium is crucial.[12–14] Then, it is essential to take the influence of turbulent medium into account in designs and applications of free-space optical communication links, and the mitigation of the turbulence effect has aroused considerable interests. Adaptive optics (AO)[15–17] is one of the effective methods to alleviating turbulence and the distorted beam profile is measured to derive a sequential error correction pattern, which is then sent through a feedback loop to the beam correction module to compensate for the beam distortion in a typical AO system. In addition, special beams with approximately non-diffracting properties, such as Bessel–Gaussian beams,[18] Hankel–Bessel beams (HB),[19] Airy vortex beams,[20] and Lommel–Gaussian beams,[21] are highly tolerant of turbulence and have been found to offer advantages over diffractive beams.

Recently, the application of the focused mirror method for alleviating turbulence effects has attracted much attention of researchers. Zhou *et al.* numerically simulated the propagation characteristics of Gaussian vortex beams with mirror and without the mirror in atmospheric turbulence and found that the former could outperform significantly the latter under the same turbulent environment.[22] Yan *et al.* investigated the crosstalk properties of focused vortex beams in atmospheric turbulence combining theoretical derivation and phase screens

[†]Corresponding author. E-mail: xg-cgb@njupt.edu.cn

© 2024 Chinese Physical Society and IOP Publishing Ltd

and found that focused LG beam is more resistant to turbulent interference than the unfocused one.[23] Wang *et al.* explored the focused mirror method and circular aperture method to reduce OAM crosstalk of LG beams in plasma turbulence and demonstrated that the focused mirror method can be used to mitigate the effects of OAM crosstalk from turbulence better than the circular aperture one.[24] Moreover, there are focused annular vortex beams,[25] focused Bessel beams,[26] and other focused vortex beams that have high tolerance to turbulent interference and potentially other properties.[27]

Compared to transport media such as atmospheric turbulence, oceanic turbulence is more complex and has a greater impact on the vortex beams passing through it. We anticipate that the performance of an LG beam with focusing mirror resisting for turbulence will have great potential applications in underwater wireless optical communication. In this paper, we study the properties of a focusing LG beam propagating in anisotropic ocean turbulence, and analyze the effect of the focusing mirror on reducing the interference of turbulent ocean through analytical derivation and numerical simulation, so as to provide useful theoretical support and reference for applications and development of underwater wireless optical communication.

In this article, the mathematical model of channel capacity based on a focused LG beam in anisotropic ocean turbulence is established. Then, the properties of the focused LG beam are studied numerically, including the influence of different light source parameters and oceanic turbulence parameters on the beam channel capacity. In addition, a comparative analysis is conducted on the system performance of underwater communication links with focused LG beams, unfocused LG beams, and HB beams, respectively.

2. Theoretical derivation

The complex amplitude of the focused LG beam at the initial plane can be expressed as[23,24]

$$E_0(\rho,\theta,0)=\Big(\frac{\sqrt{2}\rho}{\omega_0}\Big)^{m_0}L_p^{m_0}\Big(\frac{2\rho^2}{\omega_0^2}\Big)\times\exp\Big(-\frac{\rho^2}{\omega_0^2}\Big)\exp\Big(-\frac{\mathrm{i}k\rho^2}{2f}\Big)\exp(\mathrm{i}m_0\theta),\quad(1)$$

where ρ and θ represent the radial coordinate and the azimuth angle of the initial plane, respectively, m_0 is the topological charge, ω_0 is the waist radius of the beam, p is the radial index, $L_p^{m_0}(\cdot)$ is the associated Laguerre polynomial, $k=2\pi/\lambda$ is the wave number, λ is the wavelength, and f is the geometric focal length of the focusing mirror.

Then, according to the Huygens–Fresnel integral expression, we can obtain the complex amplitude of the focused LG beam at distance z in free space as

$$E_{\mathrm{free}}(r,\varphi,z)=-\frac{\mathrm{i}k}{2\pi z}\exp(\mathrm{i}kz)\int_0^{2\pi}\int_0^{\infty}E_0(\rho,\theta,0)\times\exp\Big\{\frac{\mathrm{i}k}{2z}[r^2+\rho^2-2r\rho\cos(\varphi-\theta)]\Big\}\rho\,\mathrm{d}\rho\,\mathrm{d}\theta.\quad(2)$$

Substituting Eq. (1) into Eq. (2) and utilizing the following integral formulae:[28,29]

$$\int_0^{2\pi}\exp[\mathrm{i}n\varphi-\mathrm{i}x\cos(\theta-\varphi)]\,\mathrm{d}\varphi=2\pi(-\mathrm{i})^nJ_n(x)\exp(\mathrm{i}n\theta),\quad(3)$$

and

$$\int_0^{\infty}x^{\frac{m}{2}}\exp(-px)J_m(b\sqrt{x})L_n^m(cx)\,\mathrm{d}x=\Big(\frac{b}{2}\Big)^m\frac{(p-c)^n}{p^{m+n+1}}\exp\Big(-\frac{b^2}{4p}\Big)L_n^m\Big(\frac{b^2c}{4pc-4p^2}\Big),\quad(4)$$

we can obtain

$$\begin{aligned}E_{\mathrm{free}}(r,\varphi,z)&=-\frac{\mathrm{i}k}{2\pi z}\exp(\mathrm{i}kz)\int_0^{2\pi}\int_0^{\infty}\Big(\frac{\sqrt{2}\rho}{\omega_0}\Big)^{m_0}\times L_p^{m_0}\Big(\frac{2\rho^2}{\omega_0^2}\Big)\exp\Big(-\frac{\rho^2}{\omega_0^2}\Big)\exp(\mathrm{i}m_0\theta)\\&\quad\times\exp\Big(-\frac{\mathrm{i}k\rho^2}{2f}\Big)\exp\Big\{\frac{\mathrm{i}k}{2z}[r^2+\rho^2-2r\rho\cos(\varphi-\theta)]\Big\}\rho\,\mathrm{d}\rho\,\mathrm{d}\theta\\&=-\frac{\mathrm{i}k}{2z}\exp(\mathrm{i}kz)(-\mathrm{i})^{m_0}\exp(\mathrm{i}m_0\varphi)\times\exp\Big(\frac{\mathrm{i}k}{2z}r^2\Big)\int_0^{\infty}\Big(\frac{2\rho^2}{\omega_0^2}\Big)^{\frac{m_0}{2}}\exp\Big[-\rho^2\Big(\frac{1}{\omega_0^2}+\frac{\mathrm{i}k}{2f}-\frac{\mathrm{i}k}{2z}\Big)\Big]J_{m_0}\Big(\frac{kr}{z}\sqrt{\rho^2}\Big)L_p^{m_0}\Big(\frac{2\rho^2}{\omega_0^2}\Big)\mathrm{d}\rho^2\\&=-\frac{\mathrm{i}k}{2z}\exp(\mathrm{i}kz)(-\mathrm{i})^{m_0}\exp\Big(\frac{\mathrm{i}kr^2}{2z}\Big)\Big(\frac{\sqrt{2}b}{2\omega_0}\Big)^{m_0}\times\frac{(a-c)^p}{a^{m_0+p+1}}\exp\Big(-\frac{b^2}{4a}\Big)L_p^{m_0}\Big(\frac{b^2c}{4ac-4a^2}\Big)\times\exp(\mathrm{i}m_0\varphi),\end{aligned}\quad(5)$$

where $a=(\frac{1}{\omega_0^2}+\frac{\mathrm{i}k}{2f}-\frac{\mathrm{i}k}{2z})$, $b=\frac{kr}{z}$, $c=\frac{2}{\omega_0^2}$, and $J_n(\cdot)$ is the nth order Bessel function of the first kind.

There appears to be the beam phase distortion during the beam transmission in the seawater medium due to the disturbance of oceanic turbulence, which results in the dispersion of the signal OAM mode and crosstalk between adjacent OAM modes. The complex amplitude of the focused LG beam in oceanic turbulence can be expressed as

$$E(r,\varphi,z)=E_{\mathrm{free}}(r,\varphi,z)\exp[\psi_1(r,\varphi,z)],\quad(6)$$

where $\psi_1(r,\varphi,z)$ represents the random complex phase disturbance caused by oceanic turbulence. From the superposition theory of spiral harmonics, the complex amplitude of the beam

at the receiving plane can be expressed as a superposition of beams with different OAM modes:

$$E(r,\varphi,z)=\sum_{m=-\infty}^{+\infty}a_m(r,z)\exp(\mathrm{i}m\varphi), \tag{7}$$

where the coefficient $a_m(r,z)$ is

$$a_m(r,z)=\frac{1}{2\pi}\int_0^{2\pi}E(r,\varphi,z)\exp(-\mathrm{i}m\varphi)\,\mathrm{d}\varphi, \tag{8}$$

where m denotes the topological charge corresponding to different OAM modes. By substituting Eq. (6) into Eq. (8) and in view of the statistical ensemble average of the turbulence $\langle|a_m(r,z)|^2\rangle=\langle a_m(r,z)a_m^*(r,z)\rangle$, the mode probability density of the focused LG beam with a topological charge m in oceanic turbulence is given as

$$\begin{aligned}\langle|a_m(r,z)|^2\rangle=&\frac{1}{4\pi^2}\int_0^{2\pi}\int_0^{2\pi}E_{\mathrm{free}}(r,\varphi,z)E_{\mathrm{free}}^*(r,\varphi',z)\\&\times\langle\exp[\psi_1(r,\varphi,z)+\psi_1^*(r,\varphi',z)]\rangle\\&\times\exp[-\mathrm{i}m(\varphi-\varphi')]\,\mathrm{d}\varphi\,\mathrm{d}\varphi',\end{aligned} \tag{9}$$

where * denotes the complex conjugation. The ensemble average in Eq. (9) could be given by[15]

$$\begin{aligned}&\langle\exp[\psi_1(r,\varphi,z)+\psi_1^*(r,\varphi',z)]\rangle\\&=\exp\left(\frac{-[2r^2-2r^2\cos(\varphi-\varphi')]}{\rho_0^2}\right),\end{aligned} \tag{10}$$

where ρ_0 is the transverse spatial coherence radius of a spherical wave that can be expressed as

$$\rho_0=\left[\frac{1}{3}\pi^2k^2z\xi^{-4}\int_0^{\infty}\kappa'^3\phi_n(\kappa')\mathrm{d}\kappa'\right]^{-1/2}, \tag{11}$$

here ξ is the anisotropy factor, κ' is the spatial frequency and $0<\kappa'<\infty$; $\phi_n(\kappa')$ represents the power spectrum of refractive index fluctuations in anisotropic oceanic turbulence, which can be expressed as[30]

$$\begin{aligned}\phi_n(\kappa')=&\varepsilon^{-1/3}\beta A^2\chi_{\mathrm{T}}\frac{[1+C_1(\kappa' l_0)^{2/3}]}{4\pi(\kappa'^2+\kappa_0^2)^{11/6}}\left\{\exp\left[-\frac{(\kappa' l_0)^2}{R_{\mathrm{T}}^2}\right]\right.\\&\left.+\frac{1}{\varpi^2\zeta}\exp\left[-\frac{(\kappa' l_0)^2}{R_{\mathrm{S}}^2}\right]-\frac{1+\zeta}{\varpi\zeta}\exp\left[-\frac{(\kappa' l_0)^2}{R_{TS}^2}\right]\right\},\end{aligned} \tag{12}$$

where ε is the kinetic energy dissipation rate per unit mass of fluid ranging from 10^{-10} $\mathrm{m^2/s^3}$ to 10^{-1} $\mathrm{m^2/s^3}$, χ_{T} is the dissipation rate of the mean-squared temperature and takes the value 10^{-2} $\mathrm{K^2/s}$ to 10^{-10} $\mathrm{K^2/s}$; β represents the Obukhov–Corrsin constant taking the value 0.41, the value of A is taken as 2.6×10^{-4} L/deg, C_1 is a free parameter and takes the value of 5 in this study; $\kappa_0=1/L_0$, l_0 and L_0 are the inner scale factor and outer scale factor of turbulence, respectively; ϖ indicates the ratio of the contribution of temperature and salinity to the refractive index spectrum, which ranges from -5 to 0. Q is the nondimensional constant, $R_j=\sqrt{3}(W_j-\frac{1}{3}+\frac{1}{9W_j})^{3/2}Q^{-3/2}$ $(j=\mathrm{T},\mathrm{S},\mathrm{TS})$, $W_j=\{[\frac{Pr_j^2}{(6\beta Q^{-2})^2}-\frac{Pr_j^2}{81\beta Q^{-2}}]^{1/2}-[\frac{1}{27}-\frac{Pr_j}{6\beta Q^{-2}}]\}^{1/3}$, Pr_{T} and Pr_{S} denote the Prandtl number of temperature and salinity respectively, $Pr_{\mathrm{TS}}=\frac{2Pr_{\mathrm{T}}Pr_{\mathrm{S}}}{Pr_{\mathrm{T}}+Pr_{\mathrm{S}}}$. In unsteady stratified turbulence, ζ is given as

$$\zeta=\begin{cases}1/[1-\sqrt{(|\varpi|-1)/|\varpi|}], & |\varpi|\geq1,\\1.85|\varpi|-0.85, & 0.5\leq|\varpi|\leq1,\\0.15|\varpi|, & |\varpi|\leq0.5.\end{cases} \tag{13}$$

By substituting Eq. (12) into Eq. (11), after complicated integration, we can obtain

$$\begin{aligned}\rho_0^{-2}=&\frac{\pi^3}{6\lambda^2}z\varepsilon^{-1/3}\beta A^2\xi^{-4}\chi_{\mathrm{T}}\left[\kappa_0^{1/3}U\left(2,\frac{7}{6},\frac{(\kappa_0 l_0)^2}{R_{\mathrm{T}}^2}\right)\right.\\&+\frac{1}{\varpi^2\zeta}\kappa_0^{1/3}U\left(2,\frac{7}{6},\frac{(\kappa_0 l_0)^2}{R_s^2}\right)\\&-\frac{1+\zeta}{\varpi\zeta}\kappa_0^{1/3}U\left(2,\frac{7}{6},\frac{(\kappa_0 l_0)^2}{R_{TS}^2}\right)+C_1 l_0^{2/3}\kappa_0\Gamma\left(\frac{7}{3}\right)\\&\times U\left(\frac{7}{3},\frac{3}{2},\frac{(\kappa_0 l_0)^2}{R_{\mathrm{T}}^2}\right)+C_1 l_0^{2/3}\kappa_0\frac{1}{\varpi^2\zeta}\\&\times\Gamma\left(\frac{7}{3}\right)U\left(\frac{7}{3},\frac{3}{2},\frac{(\kappa_0 l_0)^2}{R_{\mathrm{S}}^2}\right)\\&\left.-C_1 l_0^{2/3}\kappa_0\frac{1+\zeta}{\varpi\zeta}\Gamma\left(\frac{7}{3}\right)U\left(\frac{7}{3},\frac{3}{2},\frac{(\kappa_0 l_0)^2}{R_{TS}^2}\right)\right],\end{aligned} \tag{14}$$

where $\Gamma(\cdot)$ is the gamma function, and $U(\cdot)$ is the confluent hypergeometric function of the second kind.

Substituting Eqs. (5), (10) and (14) into Eq. (9) and employing the integral formula[20]

$$\int_0^{2\pi}\exp[-\mathrm{i}n\varphi+\mathrm{i}x\cos(\theta-\varphi)]\,\mathrm{d}\varphi=2\pi I_n(x)\exp(-\mathrm{i}n\theta), \tag{15}$$

we can obtain the mode probability density of focused LG beam in oceanic turbulence with topological charge m as follows:

$$\begin{aligned}\langle|a_m(r,z)|^2\rangle=&\frac{k^2}{4z^2}\left|\left(\frac{\sqrt{2}b}{2\omega_0}\right)^{m_0}\right|^2\left|\frac{(a-c)^p}{a^{m_0+p+1}}\right|^2\exp\left(-\frac{b^2}{2a}\right)\\&\times\left|L_p^{m_0}\left(\frac{b^2c}{4ac-4a^2}\right)\right|^2\exp\left(-\frac{2r^2}{\rho_0^2}\right)I_{m-m_0}\left(\frac{2r^2}{\rho_0^2}\right),\end{aligned} \tag{16}$$

where $I_n(\cdot)$ is the n-order modified Bessel function of the first kind.

Then, the probability of detecting beam mode at the receiving plane with topological charge m can be expressed as

$$P(m|m_0)=\frac{\int_0^{R/2}\langle|a_m(r,z)|^2\rangle r\,\mathrm{d}r}{\sum_{n=-\infty}^{+\infty}\int_0^{R/2}\langle|a_n(r,z)|^2\rangle r\,\mathrm{d}r}, \tag{17}$$

where R is the aperture size of the receiver. The above equation represents the signal OAM mode detection probability if

the received OAM mode m is equal to the transmitted signal mode m_0, otherwise it represents the crosstalk probability when $m \neq m_0$.

Given the smooth discrete memoryless system proposed by Shannon's information theory, according to Eq. (18), the channel capacity of the focused LG beam in oceanic turbulence can be expressed as[31–33]

$$C = \max_{P_{m_0}} [H(m_0) - H(m_0 \mid m)], \tag{18}$$

where $H(m_0)$ and $H(m_0 \mid m)$ denote the source entropy and conditional entropy, respectively, and can be expressed as

$$H(m_0) = -\sum_{m_0} P(m_0) \log P(m_0), \tag{19}$$

$$H(m_0 \mid m) = -\sum_{m} \sum_{m_0} P(m_0) P(m \mid m_0) \times \log \frac{P(m_0) P(m \mid m_0)}{\sum_{m_0} P(m_0) P(m \mid m_0)}, \tag{20}$$

where m_0 is the topological charge of the signal OAM mode varying from 0 to l_m, $N = l_m + 1$ denotes the number of transmission channels in the oceanic communication system. $P(m_0)$ denotes the probability of sending a topological charge m_0, and $P(m|m_0)$ denotes the conditional probability of receiving topological charge of $m(m \neq m_0)$. Combining Eq. (18) with Eq. (20) and utilizing the Arimoto–Blahut algorithm,[34,35] we can calculate the channel capacity of the system based on the focused LG beam in oceanic turbulence.

3. Results and discussion

In this section, the channel capacity of the focused LG beam in oceanic turbulence is analyzed by numerical simulations using the analytical formulae derived in Section 2. Unless stated otherwise, the parameters selected in this paper are $\lambda = 532$ nm, $\omega_0 = 2 \times 10^{-2}$ m, $p = 0$, $\varepsilon = 10^{-5}$ m^2·s^{-3}, $\chi_T = 10^{-8}$ K^2/s, $l_0 = 0.001$ m, $L_0 = 10$ m, $Pr_T = 0.41$, $Pr_S = 700$, $\varpi = -4$, $\xi = 2$, $N = 11$, $R = 3 \times 10^{-2}$ m, $f = 200$ m, and $z = 200$ m.

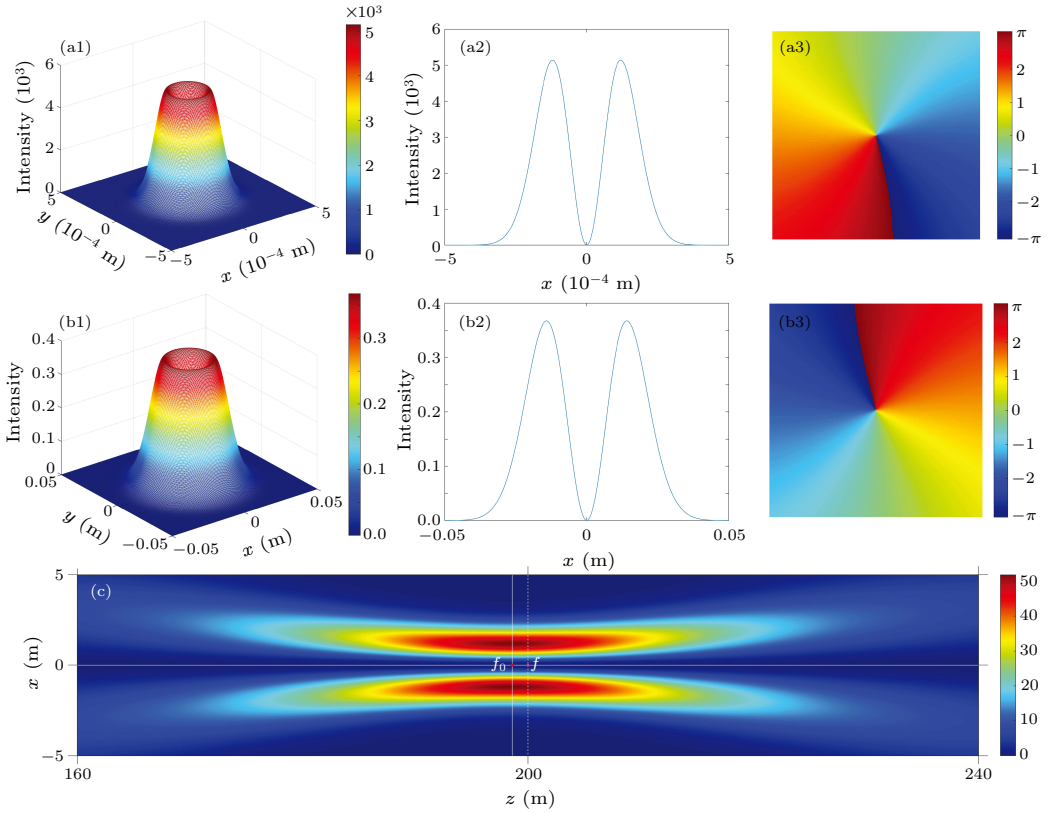


Fig. 1. Beam propagation in free space with $m_0 = 1$: (a) intensity distribution and phase distribution of the focused LG beam with $f = z = 20$ m, (b) intensity distribution and phase distribution of the unfocused LG beam with $z = 20$ m, (c) the focusing behavior of the focused LG beam with $f = 200$ m.

Figure 1 shows the intensity distribution, phase distribution and the focusing behavior of beams propagating in free space with $m_0 = 1$. When the value of the geometric focal length f is set to $+\infty$, we can obtain numerical simulation results for the unfocused LG beam. Figures 1(a) and 1(b) show the 3D intensity distribution and its cross lines ($y = 0$), together with the phase distribution of the focused LG beam (the top line) and the unfocused LG beam (the bottom line) transmitted at 20 m. As can be seen, comparing Figs. 1(a3) and 1(b3), the focusing mirror causes the beam to produce a phase burst of size π at the focal point. This phenomenon is a property of geometrical optics whose physical mechanism

originates from transverse spatial confinement, which introduces a spread in the transverse momenta through the uncertainty principle, and hence a shift in the expectation value of the axial propagation constant.[36,37] Furthermore, a comparison of the intensity distributions of two beams, as shown in the left two columns of Figs. 1(a) and 1(b), indicates that during transmission with a focusing mirror, its spatial confinement effect on the beam will concentrate the size distributions in a smaller region and significantly increase the beam intensity. On the other hand, we calculate in Fig. 1(c) the focusing behavior of the focus LG beam near the geometric focus under $f = 200$ m in the x–z plane. Here f and f_0 represent the geometric focal length and the actual focal length that correspond to the geometric focus and actual focus in free space, respectively. It is found that the intensity distribution of the focused LG beam shows a clear evolutionary process of focusing first and then diverging in the vicinity of focus. Meanwhile, the position of the maximum intensity along the propagation direction locates before the geometric focus, i.e., $f_0 < f$, and the phenomenon that the actual focal plane does not coincide with the geometric focal plane is focal shift.[38] Moreover, existing studies have shown that the size of focus shift increases with the geometric focal length or the wavelength while decreases with the waist radius.[39]

To learn about the influence of the focusing property on the channel capacity near the focus point in oceanic turbulence, we display in Fig. 2 the channel capacity versus z under different λ for the unfocused LG beam, as well as the focused LG beam with the given value of f. From Figs. 2(a) and 2(b) we can see that the channel capacity of both systems based on these two beams initially decreases with a growing z because the impact of turbulence on the beams becomes more significant with the increment of z. As z further increases, this evolutionary trend will continue to apply to the unfocused LG beam, but not to the focused LG beam with a focusing mirror. For the focused LG beam, it is clear from Figs. 2(a) and 2(b) that the capacity of the system begins to increase to the maximum and then decrease as z increases near the focus point. Notably, the value point of z corresponding to the maximum channel capacity is not exactly equal to the geometric focal length, but rather precedes it, which appears much more evident for a larger f with λ fixed in comparison between Figs. 2(b) and 2(a). Also, the difference mentioned above is more apparent with a larger λ in Fig. 2(b). Besides the influence arising from the oceanic turbulence, the physical mechanism of this result is mainly derived from the focal shift phenomenon of the focused LG beams as shown in Fig. 1(c). Nevertheless, the channel capacity of the system can still achieve high optimization at the geometric focal plane, as illustrated in Figs. 2(a) and 2(b), despite the effect of focal shift on the position of the maximum channel capacity in the vicinity of the focus, and $z = f$ is set mainly for the simulation and analysis in this paper.

One can also find from Fig. 2 that the longer the λ, the larger the system capacity because the beam with a longer λ has lower scintillation, thus bringing about a greater system channel capacity. It is worth noting that when f takes different values, the modulation effect of different λ on channel capacity varies at the geometric focus, which is much more evident in Fig. 2(b) than in Fig. 2(a). In Fig. 2(a), for the focused LG beams transmitting in the near field with short z, even though the scintillation of beams with different λ varies, their Rayleigh distance is much larger than f thus the beams all have better focusing effect,[26,39] then the interference of scintillation on beam transmission can be neglected compared to the focusing effect, so the capacity of beams with different λ tends to be the consistent. However, the focusing effect of beam gradually weakens with the increment of f, and the influence of the light intensity flicker effect on the system gradually surpasses that of the focusing effect. Therefore, as the transmission distance further increases in the far field with large z, the longer the λ, the greater the capacity of the system at the geometric focus as shown in Figs. 2(b) and 2(c). In addition, obviously, the numerical results indicate superior performance utilizing the focused LG beam compared to the unfocused one on enhancing the channel capacity under the same transmission conditions at $z = f$, due to the smaller beam size as shown in Fig. 1 and less exposure to the turbulence thus resulting in lower negative interference for using focused LG beams.

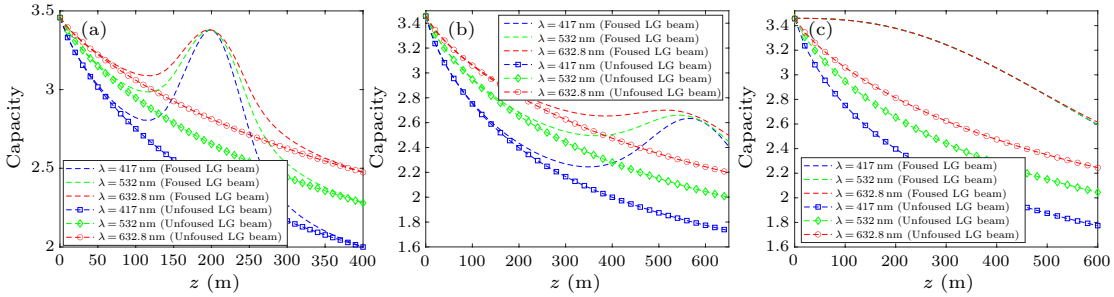


Fig. 2. The channel capacity of the unfocused LG beam, as well as the focused LG beam with (a) $f = 200$ m, (b) $f = 600$ m, (c) $f = z$ in oceanic turbulence versus transmission distance z under different wavelength λ.

Figure 3 displays the channel capacity of the focused LG beam with different waist radius ω_0 in oceanic turbulence under $f = 200$ m versus z, as well as number of transmission channels N at $z = 200$ m. As is shown in Fig. 3(a), the channel capacity of the system under different ω_0 decreases with increasing z first, and then increases as z further increases, and finally reaches the maximum before z locates at the geometric focus. Meanwhile, in the vicinity of focus, the larger the ω_0 of the focused LG beam, the greater the system channel capacity, and the closer the maximum value position to the geometric focus. This is due to the fact that the Rayleigh distance increases with the increase of ω_0, bringing about better focusing effect hence higher channel capacity of the communication link. At the same time, the larger the ω_0, the smaller the focal shift of the beam is, so the consistency between the position of the maximum channel capacity and the geometric focus is higher. On the other hand, Fig. 3(b) indicates that for given ω_0, with the increase of N, the more channels the system has to transmit information, the larger the channel capacity is.

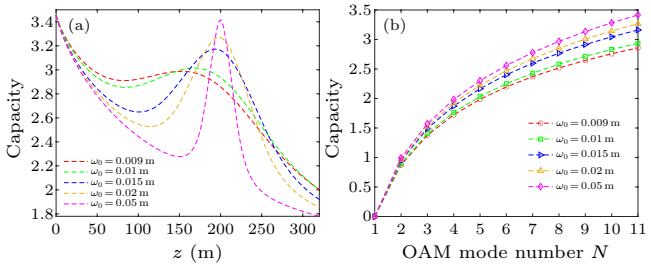


Fig. 3. The channel capacity of the focused LG beam with different waist radius ω_0 in oceanic turbulence under $f = 200$ m versus (a) transmission distance z, as well as (b) number of transmission channels N at $z = 200$ m.

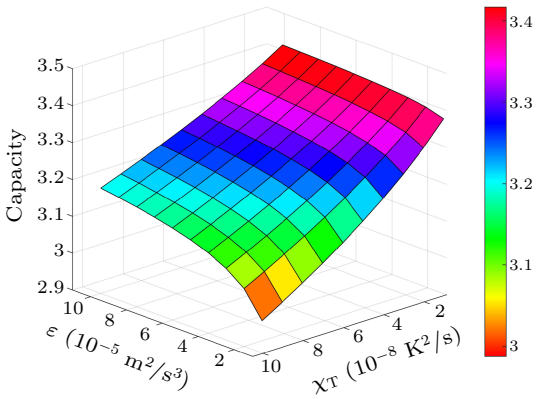


Fig. 4. The channel capacity of the focused LG beam for different dissipation rate of mean-squared temperature χ_T and dissipation rate ε of kinetic energy per unit mass of fluid.

Figure 4 shows the effect of the dissipation rate of the mean-squared temperature χ_T and the dissipation rate of the kinetic energy per unit mass of fluid ε on the channel capacity of the beam. As χ_T and ε mount, the channel capacity diminishes and increases respectively in that the turbulent intensity of seawater ascends as χ_T increases and ε decreases, magnifying the distortion of the OAM mode wavefront caused by oceanic turbulence, which reduces the channel capacity.

Figure 5 illustrates the effect of the inner scale factor l_0 and the outer scale factor L_0 on the beam channel capacity. The increase of l_0 and the decrease of L_0 augment the channel capacity. Based on oceanic turbulence theory, the turbulence with larger l_0 induces less significant beam scattering effect. A smaller L_0 of the turbulence micrifies the random deflection of the beam propagation path and consequently the beam drift, resulting in less wavefront propagation distortion and greater channel capacity, but the effect of the outer scale is not so notable.

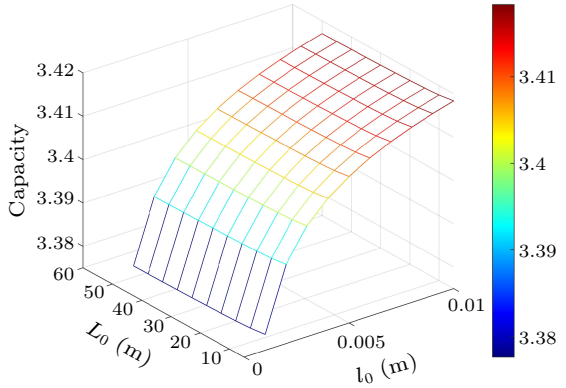


Fig. 5. The channel capacity of the focused LG beam for different inner scale factor l_0 and outer scale factor L_0.

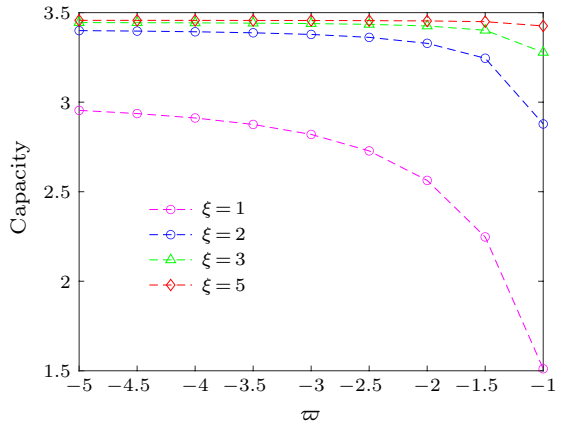


Fig. 6. The channel capacity of the focused LG beam for different anisotropy factor ξ and temperature-salinity contribution ratio ϖ.

Figure 6 demonstrates the impact of anisotropy factor ξ and temperature-salinity contribution ratio ϖ on the channel capacity of the focused LG beam. The channel capacity wanes with a larger ϖ because the salinity fluctuations of seawater have a greater perturbation effect on the capacity than temperature fluctuations. On the other hand, the anisotropic unstable stratified oceanic turbulence power spectrum degenerates to isotropic when ξ is equal to 1. For ξ, the larger its value, the stronger the anisotropy and the greater the channel capacity of the beam mainly because higher anisotropy of the turbulent flow minimizes the refractive fluctuations of the beam and

amplifies the transmission effect, leading to less interference in the oceanic channel and a larger system capacity.

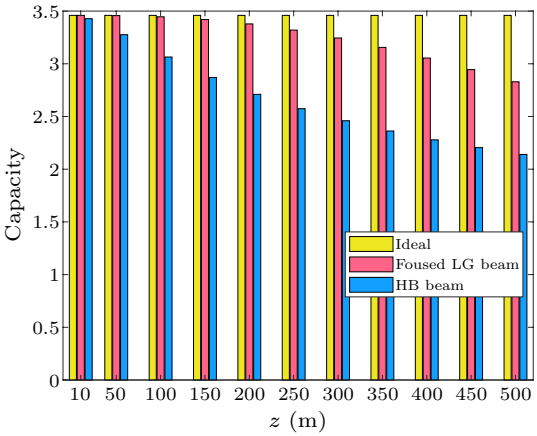


Fig. 7. Channel capacity as a function of z with the focused LG beams and the HB beams.

The comparison of the system channel capacity based on the focused LG beam, the HB beam with diffraction-free characteristics and the ideal condition is depicted in Fig. 7. We can see that when the transmission distance is given, the channel capacity of the system based on the focused LG beam and the HB beam is smaller than that of the system under ideal condition due to the interference of turbulence effect. On the other hand, under the same transmission conditions, the channel capacity of the HB beam-based system decreases more sharply with increasing transmission distance than that of the focused LG beam, indicating that the focusing mirror can effectively mitigate the effect of oceanic turbulence and augment the channel capacity of OAM-based underwater optical communication systems.

4. Conclusion

In summary, we have numerically analyzed propagation and properties of a focused LG beam in anisotropic turbulent ocean. The impacts of turbulent ocean parameters and beam source parameters on the channel capacity of the underwater communication link are discussed in detail. The results indicate that the LG beam with mirror has a smaller beam size and higher intensity density during transmission, resulting in strong anti-turbulence and anti-attenuation performance owing to modulation of the focusing mirror. Meanwhile, for the focused LG beam, the location of the maximum channel capacity in the propagation direction is not consistent with the location of the geometric focal plane where the system can still achieve a high degree of optimization for the channel capacity. In addition, it is found that the greater the wavelength or the beam waist radius, and the larger the number of transmission channels applicable to improve the channel capacity for long distance transmission. Further, the capacity of the system increases with the mount of the kinetic energy dissipation rate per unit mass of fluid, the inner scale of seawater turbulence and the anisotropy factor, and decreases with the increase of the mean-squared temperature dissipation rate of oceanic turbulence, temperature-salinity contribution ratio and turbulent outer scale factor. In comparison of the non-diffraction HB beam and the unfocused LG beam, the focused LG beam has larger capacity due to its less beam spreading in the underwater channel. This provides a reference for designs of more robust OAM-based underwater optical communication links.

Acknowledgements

This work was supported by the Science and Technology Innovation Training Program of Nanjing University of Posts and Telecommunications (Grant No. CXXZD2023080), the National Natural Science Foundation of China (Grant Nos. 61871234 and 62001249), the Natural Science Foundation of Nanjing University of Posts and Telecommunications (Grant No. NY222133), and the Open Research Fund of National Laboratory of Solid State Microstructures (Grant No. M36055).

References

[1] Allen L, Beijersbergen M W, Spreeuw R J C and Woerdman J P 1992 *Phys. Rev. A* **45** 8185
[2] Zhan H C, Chen B, Peng Y X, Wang L, Wang W N and Zhao S M 2023 *Chin. Phys. B* **32** 044208
[3] Guo H X, Qiu X D and Chen L X 2023 *Appl. Phys. Lett.* **122** 061103
[4] Guzmán E A and Arzola A V 2022 *J. Opt. Soc. Am. B* **39** 1233
[5] Chen K, Ma Z Y and Hu Y Y 2023 *Chin. Phys. B* **32** 024208
[6] Bao X J, Zhu Y, Wang J C and Hu Z D 2014 *Phys. Scr.* **98** 035101
[7] Yu J J, Zhang P, Ruffato G and Lin D 2022 *Front Phys.* **10** 1026004
[8] Willner A E 2021 *Opt. Photon. News* **32** 34
[9] Willner A E, Zhao Z, Liu C, Zhang R Z, Song H Q, Pang K, Manukyan K, Song H, Su X Z, Xie G D, Ren Y X, Yan Y, Tur M, Molisch A F, Boyd R W, Zhou H B, Hu N Z, Minoofar A and Huang H 2021 *APL Photon.* **6** 030901
[10] Yang H B, Yan Q Z, Wang P, Hu L F and Zhang Y X 2022 *Opt. Express* **30** 9053
[11] Ma W Q, Lu H M, Chen D Y, Jin J L and Wang J P 2022 *J. Opt.* **24** 065701
[12] Nikishov V V and Nikishov V I 2000 *Int. J. Fluid Mech. Res.* **27** 82
[13] Lu L, Ji X L and Baykal Y 2014 *Opt. Express* **22** 27112
[14] Wang H, Kang F Z, Wang X, Zhao W and Sun S W 2021 *Chin. Phys. B* **30** 064207
[15] Chang H, Yin X L, Yao H P, Wang J J, Gao G, Xin X J and Guizani M 2022 *IEEE Trans. Wireless Commun.* **21** 11151
[16] Zhan H C, Wang L and Wang W N 2022 *J. Lightwave Technol.* **40** 4129
[17] Pang B Q, Wang S, Cheng T, Kong Q F, Wen L H and Yang P 2017 *Chin. Phys. B* **26** 054204
[18] Wang A T, Yu L H, Li J F and Liang X Y 2023 *Chin. Phys. B* **32** 044201
[19] Yin X L, Guo Y L, Yan H, Cui X Z, Chang H, Tian Q H, Wu G H, Zhang Q, Liu B and Xin X J 2018 *Acta Phys. Sin.* **67** 114201 (in Chinese)
[20] Wang X G, Yang Z and Zhao S M 2019 *Optik* **176** 49
[21] Yu L and Zhang Y 2017 *Opt. Express* **25** 22565
[22] Zhou M Y, Zhou Y Q, Wu G F and Cai Y J 2019 *Opt. Express* **27** 10280
[23] Yan J L, Wei H Y, Cai D M, Jia P and Qiao T Z 2020 *Acta Phys. Sin.* **69** 144203 (in Chinese)
[24] Wang Y K, Bai L, Zhang D M, Xie J Y, Guo Y and Guo L X 2021 *IEEE Photon. J.* **13** 1

[25] Cao J X, Liang H J, Zhou Y Q, Wu G F and Pang X Y 2022 *Front. Phys.* **10** 1013729
[26] Wei H Y, Yan J L, Jia P and Cai D M 2020 *Acta Opt. Sin.* **40** 2401001 (in Chinese)
[27] Qin Y, Yang H J, Jiang P, Caiyang W N, Zhou M G and Zhou Y F 2023 *Optik* **272** 170286
[28] Wang S L, Cheng M J, Yang X H, Xu J P and Yang Y P 2023 *Opt. Express* **31** 20861
[29] Kotlyar V V, Khonina S N, Almazov A A and Soifer V A 2006 *J. Opt. Soc. Am. A* **23** 43
[30] Li Y, Zhang Y X and Zhu Y 2019 *Opt. Express* **27** 7656
[31] Li Y X, Cui Z W, Han Y P and Hu Y F 2019 *J. Opt. Soc. Am. A* **36** 471
[32] Wang S L, Yang D H, Zhu Y and Zhang Y X 2021 *Appl. Opt.* **60** 4135
[33] Wang X G, Wang L and Zhao S M 2021 *Appl. Opt.* **60** 8321
[34] Arimoto S 1972 *IEEE Trans. Inf. Theory* **18** 14
[35] Blahut R 1972 *IEEE Trans. Inf. Theory* **18** 460
[36] Boyd R W 1980 *J. Opt. Soc. Am.* **70** 877
[37] Feng S M and Winful H G 2001 *Opt. Lett.* **26** 485
[38] Zhang M H, Chen Y H, Liu L and Cai Y J 2016 *J. Mod. Optic.* **63** 2226
[39] Ren Z C, Qian S X, Tu C H, Li Y N and Wang H T 2015 *Opt. Commun.* **334** 156